

# Aquifer recharge capacity assessment of an anthropogenically impacted wetland by the DC resistivity geophysical method

César Augusto Moreira<sup>1</sup>  · Vania Silvia Rosolen<sup>1</sup>  · Marco Antonio Foutoura Hansen<sup>2</sup>  · Henri Masquelin<sup>3</sup>  · Rogério Mota<sup>4</sup> 

Received: 14 January 2023 / Accepted: 26 March 2023

Published online: 11 April 2023

© The Author(s) 2023 [OPEN](#)

## Abstract

Population growth and social and economic development demand increasing volumes of water for public supply, especially in scenarios where surface sources such as rivers may not meet the basic demands for the population. In southeastern Brazil, with emphasis on the Piracicaba region, there is a conflict over water use regarding agricultural and industrial activities, where the sugar-alcohol sector is widely highlighted. The region has thousands of hectares of sugarcane cultivated, which requires intensive use of fertilizers and pesticides, in addition to the need for large volumes of water in the production of sugar and ethanol, where the main effluent produced is represented by vinasse, used as fertilizer complement and soil hydration in sugarcane fields. This work presents the results of a geophysical diagnosis in a closed wetland, located in a sugarcane field region, to evaluate the hydrogeological function of this environment in aquifer recharge and the risks that land use can cause in the quality and availability of surface and underground water resources. The geophysical survey consisted of nine lines of electrical resistivity tomography in Schlumberger arrangement, submitted to 2D processing and inversion followed by interpolation and generation of 3D visualization models. The results indicate a direct connection between water accumulated in the wetland and the aquifer underneath, separated by an aquitard interface about 44 m thickness. The study points out to the high vulnerability to the input of pesticides and vinasse effluent from the surrounding sugarcane fields to the interior of the wetland, given the absence of riparian forest or buffer zone, in addition to the risk of contamination of surface and groundwater. Understanding the local hydrological dynamics should subsidize the sustainable use of the soil providing preservation of water resources, with emphasis on aquifers, a source of increasing importance in the face of the imminent scarcity of surface resources.

**Keywords** Wetland · Sugar cane · Vinasse · Geophysics · ERT · Aquifer

## 1 Introduction

Population growth and the expansion of urban centers combined with the stimulation of agricultural activities with an emphasis on export commodities, imply increasing pressure on water resources. In southeastern Brazil, there are several urban centers that faces water crises and imbalances between the supply of water resources and the demand for public supply and other uses, with prolonged periods of rationing or intermittent supply [1–8].

✉ César Augusto Moreira, cesar.a.moreira@unesp.br | <sup>1</sup>Department of Geology, São Paulo State University (Universidade Estadual Paulista), Av. 24A, 1515, Rio Claro, SP 13506-900, Brazil. <sup>2</sup>Pampa Federal University, Av. Pedro Anunciação, 111, Caçapava do Sul, RS 96570-000, Brazil. <sup>3</sup>Instituto de Ciencias Geológicas, Universidad de la Republica, Iguá 4225 Esq. Mataojo, 11400 Montevideo, Uruguay. <sup>4</sup>National Laboratory for Civil Engineering, Avenida do Brasil, 101, 1700-066 Lisbon, Portugal.



Intensive agriculture, directly (irrigation) or indirectly (deforestation and introduction of monocultures), demands increasing amounts of water, particularly in Brazil, which stands out for the export of agricultural commodities. The country is the world's largest sugarcane producer and in the 2020/21 harvest, it was responsible for the production of 654.5 million tons destined to produce 41.2 million tons of sugar and 29.7 billion liters of ethanol [9]. This agroindustry involves a complex chain of activities, starting with land preparation and planting, followed by harvesting and processing in large industrial complexes [10]. In these plants, after the sugar and biofuel processing, part of the effluent generated, called vinasse, is released into the sugarcane fields as a partial substitute for soil irrigation and supplementary fertilizer. For each liter of alcohol produced in the plants, 10 to 15 L of vinasse are produced, one of the major justifications for its large use in fertigation systems in sugarcane fields [11].

The state of São Paulo leads Brazilian production and accounts for 54.1% of the quantity produced in the 2020/21 harvest, responsible to production of 48.4% of ethanol (14.3 billion liters) and 63.2% of sugar (26.0 million tons) [9]. This activity has a positive impact on state revenue, in addition to generating thousands of direct and indirect jobs, with clear economic and social benefits. On the other hand, agricultural management is based on the use of large and growing volumes of mineral-based fertilizers and pesticides, which is great for the soil.

Regarding vinasse, the liquid resulting from the fermentation of sugarcane, it is an effluent composed of large amounts of potassium, sulfur, phosphorus, nitrogen, calcium, magnesium, and micronutrients, which is great for the soil [12]. On the other hand, it can cause severe impacts on the environment because it has a high Biochemical Oxygen Demand (BOD) and high acidity, resulting in the depletion of dissolved oxygen (DO) in water [13]. The occasional supply of vinasse in environments of high environmental sensitivity such as wetlands, springs, and rivers, put the flora, fauna and the quality of the water resource at risk [14–21].

Wetlands are particularly sensitive environments in this scenario, as they consist of, from a geomorphological point of view, depressions in closed reliefs and with accumulation of water in the lower portion, either permanently or intermittently [22, 23].

These closed basins generally have a gentle slope and are systematically incorporated by agriculture crops. Its hydrogeomorphological configuration provides the input of several agrochemicals carried by surface flow in periods of rain. Several studies demonstrate the function of wetlands as a surface water resource, in addition to being a connection or aquifer recharge zone, a condition that reveals their importance in the maintenance of subsurface water resources [24–31].

The current paradigm regarding the universalization of basic sanitation in the countryside of the State of São Paulo implies into the increasing access to rivers and groundwater resources, preservation of recharge zones, springs and rivers, combined with the management and rational use of land on an ongoing basis by sugar cane monoculture. The search for environmental sustainability of agricultural activities of great economic and social relevance implies scientific studies with a view to understand systems and processes in sensitive environments and the search for technical alternatives to reduce environmental impacts [32–37].

Geophysical studies can contribute to the understanding of hydrogeological dynamics, recognition of recharge zones and main flow paths, in addition to the recognition of appropriate locations for drilling wells or diagnosis of contaminated areas [38–48].

This study consists of a geological and geophysical diagnosis of a closed wetland located in a sugarcane monoculture area with the objective of evaluating the hydrological function of this environment, specifically as a connection area between the surface and the subsurface as a recharge zone. The study also evaluates the risk of contamination in the long term by the input of agrochemicals.

## 2 Material and methods

### 2.1 Study area

The study area is in the district of Tanquinho, about 19 km north of the municipality of Piracicaba, in the countryside of the State of São Paulo, Brazil (Fig. 1). The regional climate is classified as Cwa according to Köppen's climate classification. It has high rainfall rates in the summer (from October to March) and dry season in winter (from April to September). It presents an average annual rainfall of 1500 mm and an average annual temperature of 21.9 °C.

The area is in the Corumbataí river hydrographic watershed, management by the Water Resources Management Unit of the rivers Piracicaba, Capivari and Jundiá rivers (UGRHI-PCJ). This management unit is highly urbanized and industrialized and the use of rural land is strongly focused on sugarcane monoculture, concentrated in an area of

approximately 15,414 km<sup>2</sup>. Covering 76 municipalities and a population of 5.85 million people, the area is responsible for 7% of the Brazilian Gross Domestic Product (GDP) and 17% of the GDP of the State of São Paulo [49].

The study area is about 700 m away from the nearest drainage and about 4 km from the Corumbataí river. This river is of fundamental importance for the municipalities of Rio Claro and Piracicaba, as it represents the main source of water collection for public supply of an estimated population of 666,000 people. The use of water in this region is distributed in 54% urban, 26% in agriculture and 20% by industries. The demand for urban supply in 2020 was 2.6m<sup>3</sup>/s while global usage (urban, agriculture/livestock and industry) was 4.4m<sup>3</sup>/s. The historical series shows the minimum flow of the Corumbataí River is around 5m<sup>3</sup>/s, an index close to the current integrated demand and insufficient for the projected growth for the coming years [49–51].

The study site consists of a closed wetland with a partially circular shape, 500 m long and 340 m wide. The flooded area changes according to the period of the year: it reaches a maximum area of approximately 128,000 m<sup>2</sup> at the end of the rainy season in April and drops substantially at the end of the dry season in September. The entire surroundings are occupied by extensive sugarcane monoculture, up to the maximum flooding limit of the wetland, separated by a rural road (Fig. 2).

On the boundary of wetland, the dark grey soil is clayey to silt-clayey with higher contents of sand fraction (quartz grain) in the topsoil and higher silty texture in the saprolite. The relief around the topographic depression (humid area) has a soft slope, with topographic variations between 644 m (center base of the humid area) and 652 m (highest portion and water divider), which configures a watershed with an area of approximately 630,000m<sup>2</sup> (Fig. 3).

The local geological context is represented by sedimentary rocks of the Irati and Tatuí Formations (Fig. 3), constituent units of the Paraná Sedimentary Basin, defined as an extensive intracratonic basin established on the South American Platform, reaching about 6,000 m of sediments and basaltic spills. This sedimentary province is situated in the central-eastern part of South America, covering about 1,700,000km<sup>2</sup> in Brazil, Argentina, Uruguay and Paraguay [52, 53].

The Irati Formation constitutes the bedrock of the wetland, represented by the Taquaral (lower) and Assistência (upper) Members, with maximum thickness of 70 m [54]. The Taquaral Member is represented by gray siltstone and dark greenish-gray shales. The Assistência Member presents dark pyrobetuminous shales intercalated with dolomitic limestones and subordinate pelites, with the presence of silica nodules and stromatolites. The occurrence of thicker layers of dolomitic limestone at the base of the Assist Member has promoted the establishment of several mining companies in the study region [52]. The proposed sedimentation environment for the Irati Formation occurred in calm marine waters for the Taquaral Member and shallow-water platform marine for the Assistência Member [52]. The age of the Irati Formation was established by [55], with geochronological dating of zircons in volcanic ash as Lower Permian.

The Tatuí Formation is composed predominantly of sandy siltstones and siltstones, with minor intercalations of carbonate rocks, sylexites and sandstones. Regarding its lithotypes, [56] suggested for the Tatuí Formation a division into two distinct sedimentary packages: lower consisting mostly of purplish brown and greenish yellow siltstones, and upper consisting of gray and yellowish siltstones. [57] states that the lithotypes of the Tatuí Formation are indicators

**Fig. 1** Location of the study area

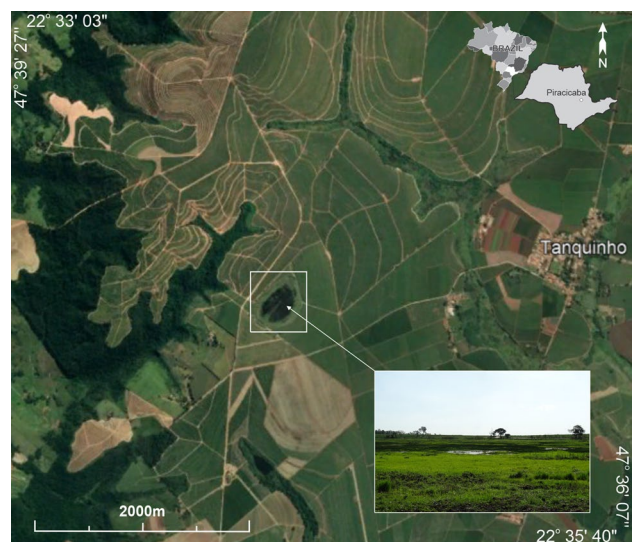




**Fig. 2** Set of images of the study area, with panoramic image, limits with sugarcane area, and details of the flooded region



**Fig. 3** Topographic elevations of the wetland area and upper limit of the basin, with geological contact of the Irati Formation (upper) and Tatuí Formation (lower)





of a transgressive marine environment with the influence of anastomosing rivers with high sediment load, besides the occurrence of fan-delta complexes.

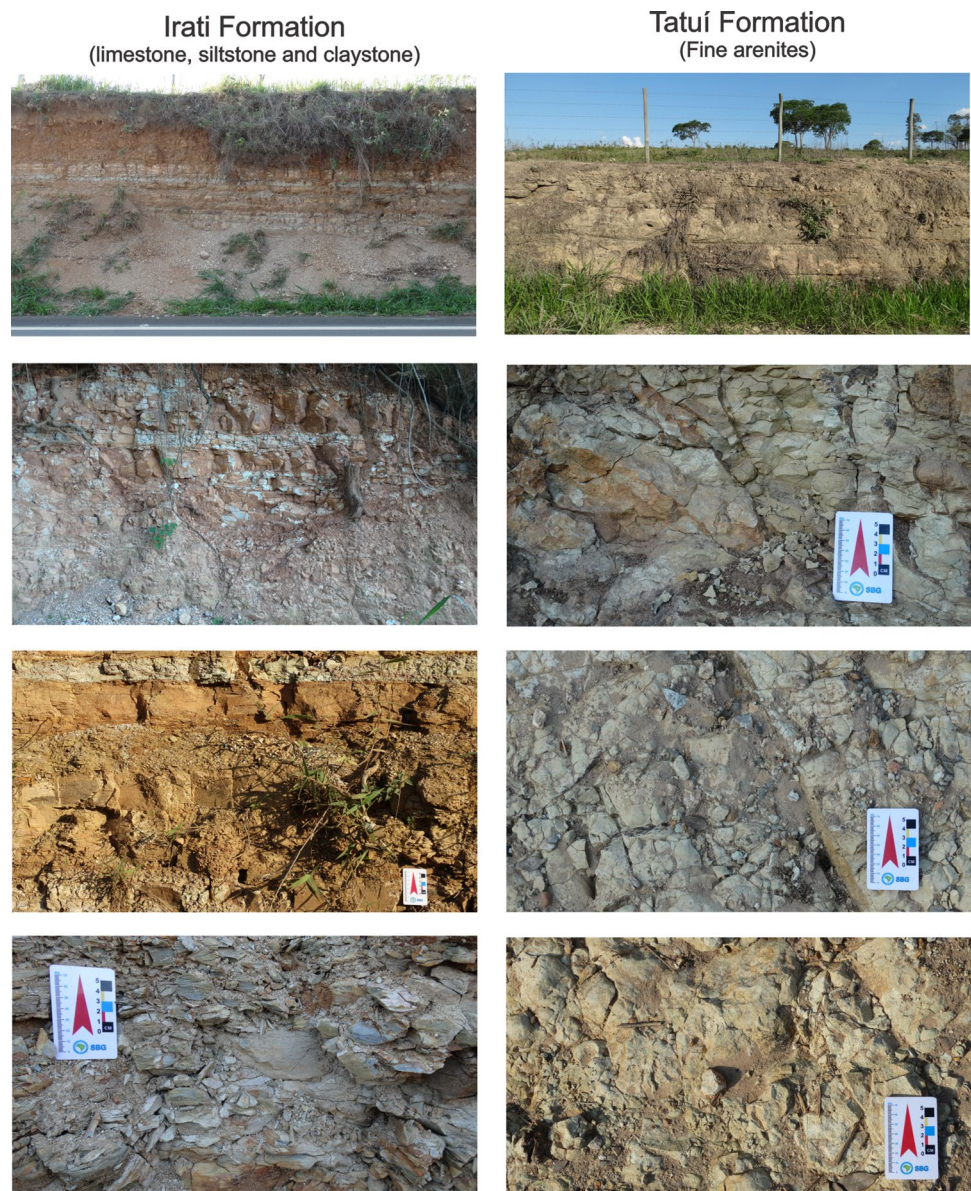
Locally the Irati Formation is represented by the Taquaral Member in basal contact with sediments of the upper portion of the Tatuí Formation (Fig. 4).

The hydrogeological context of the region classifies the geological units into two distinct aquifer systems: Passa Dois Aquiclude (Corumbataí and Irati Formations) and Tubarão Aquifer (Tatuí Formation and Itararé Group).

The Passa Dois Aquiclude is a sedimentary hydrogeological unit of regional extension that separates the Tubarão and Guarani Aquifers. This aquiclude is formed by sediments deposited in marine environments, with lithologies predominantly represented by shales, siltstones, argillites, limestones and dolomites that occur as layers with different thicknesses, sometimes rhythmically intercalated. Due to the constitution of mostly fine granulation, it has low aquifer capacity and insufficient productivity for the supply of large communities, although it presents flow in fractured systems and aquitard characteristics and considerable productivity, especially in the Irati Formation [58].

The Tubarão Aquifer is a sedimentary aquifer of regional extension and with occurrences up to 2000 m deep. Due to its large, confined extent and relatively low productivity compared to other sedimentary aquifers, the Tubarão Aquifer is predominantly exploited in the outcropping area, as in the study region. It is composed of sediments deposited in glacial, continental and marine environments. The lithologies are quite heterogeneous and represented by siltstones,

**Fig. 4** Representative lithotypes of the Irati (left) and Tatuí (right) Formations for the study region



argillites, shales, diamictites, very fine sandstones to conglomeratic and rhythmites that occur as layers with different thickness, intercalated and discontinuous. The aquifer presents a low productivity, where sustainable flows are below  $10\text{m}^3/\text{h}$  per well. Localized occurrences of sandier lithologies, eventually associated with rock fracturing, are responsible for higher water productivity, whose recommended sustainable flow rates can reach up to  $40\text{m}^3/\text{h}$ . In general, the water from the Tubarão Aquifer is of satisfactory quality for human consumption, although it has relatively high levels of sodium, fluoride and sulfate [58].

## 2.2 Data acquisition

The geophysical survey involved the DC resistivity method by means of Electrical Resistivity Tomography (ERT) with 6 lines with 420 m each, 10 m electrode spacing, acquired in Schlumberger arrangement (Fig. 5). The DC resistivity methods are based on the principle that the electric potentials (voltages) measured around a current-carrying electrode are affected by the electrical resistivities of the underlying materials [59].

The applicability of DC resistivity in geological investigations lies in the potential for discrimination of a wide range of rocks from the physical parameter electrical resistivity, in addition to the wide contrast of resistivity between dry rocks (highly insulating) and wet rocks (highly conductive), a condition that enables robust indirect hydrogeological studies with a high degree of detail [60].

The positioning and orientation of the lines aimed to cover both the interior of the wetland and part of the surrounding land used for sugarcane planting. Lines 1 and 6 were oriented in the  $\text{N}42^\circ$  direction, while the remaining lines were oriented in the  $\text{N}127^\circ$  direction.

The geophysical equipment used was the Terrameter LS, manufactured by ABEM Instrument (Sweden). This equipment consists of a single automated module for transmitting and receiving data based on prior programming of the acquisition parameters (Fig. 6). The device 250W of power, with a maximum current of 2.5 A and resolution of  $1\ \mu\text{V}$  [61]. The equipment was calibrated for 10 alternating cycles of electric current injection between electrodes and potential difference reading in each measurement, with a quality factor limited to 4% of average value variation. The equipment performs previous measurements of contact resistance before and during data acquisition, in order to verify the integrity of the connections between electrodes and cables for signal transmission and reception.

The data treatment process was made through the Res2dinv program, designed to invert large data sets, collected from the electrode positions along the survey line, to automatically generate a two-dimensional (2D) resistivity model for the subsurface [62]. The Res2dinv uses the smoothed inversion routine based on the smoothness-constrained least-squares method.

The 2D data were processed using the basic routine of the Res2Dinv software. A forward modeling subroutine is used to calculate the apparent resistivity values, and a non-linear least-squares optimization technique is used for the repeated inversion routine, used for calculating resistivity. As a result, 2-D resistivity inversion models are obtained with

**Fig. 5** Arrangement of electrical resistivity tomography lines

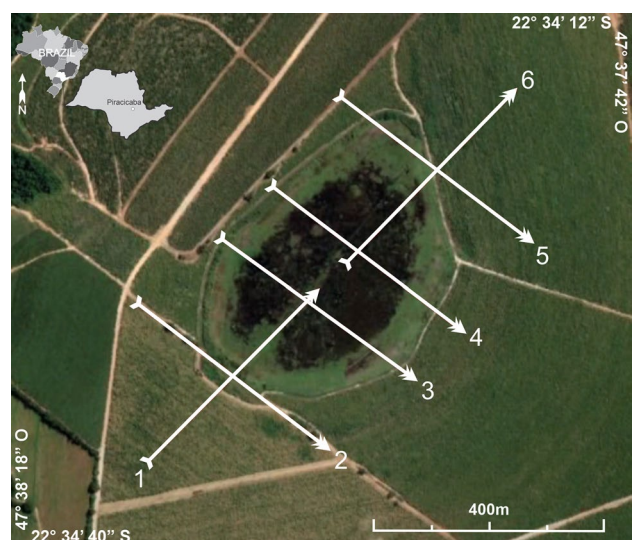






**Fig. 6** Geophysical data acquisition, with panoramic view of the from the end of the electric tomography line (left) and detail of the equipment in operation (right)

surface distance and vertical depth. The resistivity values are presented on a logarithmic scale, which extrapolates and highlights the contrasts. These interpolation intervals are organized on a color scale [63].

The 2-D inversion data is plotted on a spreadsheet to obtain the pseudo-3D visualization models. The spreadsheet must contain the variables,  $x$ —geographic position of the readings along the acquisition lines,  $y$ —spacing between lines,  $z$ —depth by inversion, and  $R$ —resistivity value. The pseudo-3D model is generated on the Oasis Montaj platform, in which the data acquired by the 2-D inversion model are interpolated and through the minimum curvature method, and then pseudo-3D visualization models are produced. A pseudo-3D visualization model is a tool that allows cuts by the depth levels. By these tools, it is possible to understand areas with complex geological structures and, particularly hydrological studies, as it determines the level of soil saturation, preferential flow paths, aquifer geometry, and hydraulic properties, important information for shaping conceptual models of hydrogeological systems. This methodology of processing the data has already been used in other studies with different objectives [28, 44, 48, 64–66].

### 3 Results and discussion

The initially processed data were evaluated individually in terms of the RMS deviation, which varied from 3.4 to 5.3, which can be attributed to the contrast of electrical properties in each section, which is conditioned to geological factors and degree of saturation in water.

A single scale of values was elaborated, varying between  $10\Omega\cdot\text{m}$  and  $500\Omega\cdot\text{m}$ , and applied to all inversion models with the aim of providing a basis for comparison. Inversion models are presented with topographic correction and vertical exaggeration fixed at 1x.

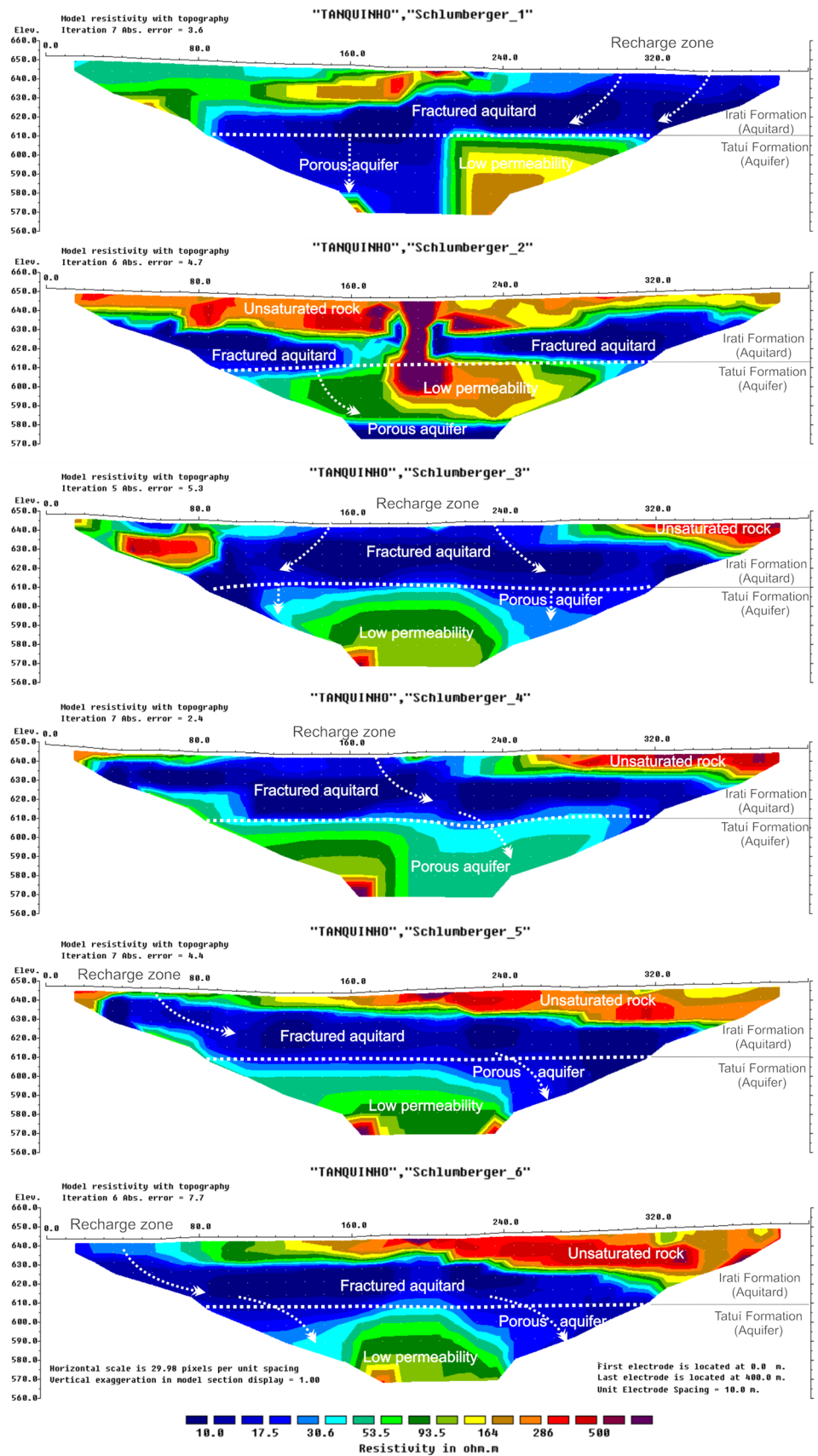
Line 1 was planned so that its initial half covered the sugarcane cultivation area, and the final half covered the humid area, with orientation towards  $N125^\circ$ . This section presents resistivity values between  $100\Omega\cdot\text{m}$  and  $500\Omega\cdot\text{m}$  corresponding to Irati Formation in its initial half, indicative of dry or low moisture soil and rock. The final half of the section has a wide range of resistivity with below  $50\Omega\cdot\text{m}$ , which basically corresponds to the entire coverage of the wetland, indicative of completely saturated soil and rock (Fig. 7).

This saturated zone has a wide lateral extension and a trend of vertical continuity towards the interior of the Tatuí Formation, indicative of a direct connection between the accumulated water of the wetland and the Tubarão aquifer.

In the range of Tatuí Formation there is a vertical contact between different resistivity areas: the initial half with values lower than  $50\Omega\cdot\text{m}$  and the final half with values between  $100\Omega\cdot\text{m}$  and  $250\Omega\cdot\text{m}$ . This contrast of values for the same geological unit is evidence of faciological variation, described in sedimentological studies of this unit, which indicate a clear permeability variation, where low values represent porous and permeable rocks, while high values are indicative of low porosity rocks and permeability. It is remarkable the coincidence between the zone of low permeability in Tatuí Formation and the boundary of the wetland, a reflection that these rocks act as a support substrate for the saturated range of Irati Formation and the surface wetland itself (Fig. 7).

Line 2 crosses line 1 perpendicularly and with coincident centers, however, line 2 was positioned outside the current flooding zone of the wetland, with orientation towards  $N45^\circ$ . This section presented a shallow horizontal layer of high

**Fig. 7** Inversion models of lines 1 to 6, with emphasis on recharge zones, groundwater flow and contact between geological/aquifers units





resistivity (above 300 $\Omega$ .m) characterized as a horizon of dry soil and rock, with a maximum thickness of 20 m. Between 20 and 45 m there is a horizontal layer of low resistivity (below 50 $\Omega$ .m), indicative of rock completely saturated in water, divided in the center of the section by a vertical zone of high resistivity (above 500 $\Omega$ .m), possibly related to a siliceous or impermeable silicified limestone, existing materials in Irati Formation (Fig. 7).

This fractured aquifer horizon has horizontal basal contact with a layer that varies from the center to the end of the section, with moderate to high resistivity (above 150 $\Omega$ .m), indicative of a horizon of low permeability. The interval of this layer from the center to the beginning of the section presents low resistivity values (below 100 $\Omega$ .m) until the base of the section, which presents resistivity values below 50 $\Omega$ .m, indicative of an aquifer zone that connects the upper fractured aquifer with the lower porous aquifer. This interval of resistivity value of 100 $\Omega$ .m must represent a siltstone variation of the Tatuí Formation, with moderate permeability, but which connects two rocks of high permeability (Fig. 7).

Lines 3 and 4 cross the interior of the wetland and are almost completely positioned inside, oriented parallel to line 2 and with the data acquisition direction N45°. In the shallow lateral limits of both sections there are horizontal layers of high resistivity (above 250 $\Omega$ .m), which reflect horizons of dry soil and rock. In both lines there is a wide horizontal band of low resistivity (below 50 $\Omega$ .m) from the surface to the 610 m elevation (Fig. 7). This electrical resistivity pattern is a clear indicator of surface water infiltration towards the interior of the Irati Formation rocks. Below the 610 m elevation there is an increase in electrical resistivity (around 100 $\Omega$ .m), indicative of changes in the porosity and permeability of the rock, represented by fine sandstones of Tatuí Formation, in horizontal contact with the upper unit. In both lines there are indications of water infiltration from the Irati Formation (aquitard) to the Tatuí Formation (aquifer).

Lines 5 and 6 are very similar in terms of results. However, line 5 is oriented parallel to lines 2, 3 and 4, with the center positioned at the NE limit of the wetland, covering the sugarcane area in its final portion and covering the wetland in its initial portion. Line 6 has a similar orientation to line 1, but with the initial half inside the wetland, the center positioned at the wetland/cane field interface and the final half in the sugarcane field, in addition to the data acquisition direction for N45°.

In the shallow initial portion of both sections there is a horizon of low resistivity (below 50 $\Omega$ .m) which follows in the form of an extensive horizontal layer with basal contact at elevation 610 m (Fig. 7). This pattern indicates a zone of surface water infiltration from the wetland into the interior of the Irati aquitard through fractures. This basal interface consists of contact with fine sandstones of Tatuí Formation, characterized by a wide range of moderate resistivity (100 $\Omega$ .m) and low permeability, an interface that supports the wetland. A smaller range of low resistivity (below 50 $\Omega$ .m) indicates the connection between the aquitard with the Tatuí aquifer (Fig. 7). In the shallow horizon of both sections there are extensive layers of high resistivity (above 250 $\Omega$ .m) that characterize dry soil and rock, predominantly in sugarcane plantation areas.

The lateral interpolation of the set of geophysical lines allowed the modeling of electrical resistivity maps for 6 different levels or elevations: 640 m, 630 m, 620 m, 610 m, 600 m and 590 m (Fig. 8).

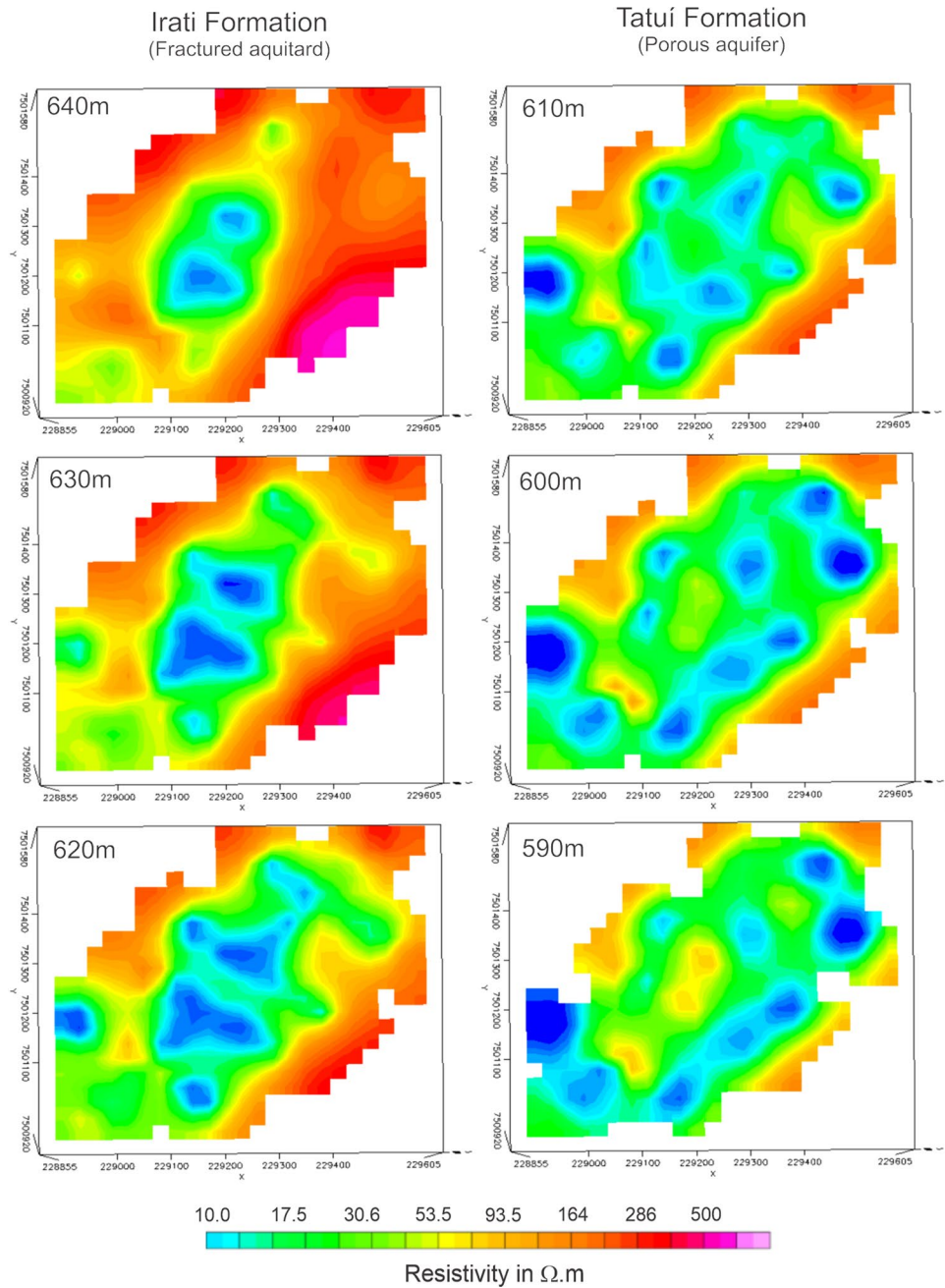
The map with an altitude of 640 m corresponds to a depth of 4 m, where values below 50 $\Omega$ .m configure an area with an identical shape of the area with greater saturation into the wetland (Fig. 3). It corresponds to the beginning of the rock layer, which must consist of a surface of low permeability, a factor that justifies the existence of water accumulated on the surface and justifies the existence of permanently humid terrain.

However, within this area there are two smaller and independent areas, with a maximum resistivity of 13 $\Omega$ .m, which must represent two independent systems of fractures in the siltstones and limestones of the Irati Formation, which correspond to the main zones of infiltration of water accumulated in the wetland towards the interior of the rock (Fig. 8). Apparently, there is a balance between the volume of water accumulated throughout the year and the rate of vertical infiltration, since the geophysical survey was carried out at the end of the regional dry period to facilitate field work, and at the time most of the local soil presented saturation and humidity.

The maps of 630 m and 620 m of altitude correspond respectively to 14 m and 24 m of depth and are characterized by presenting an increasing amplification of areas with resistivity lower than 13 $\Omega$ .m (shades of blue) and between 13 $\Omega$ .m and 50 $\Omega$ .m (shades of green), described for the 640 m altitude map (Fig. 8). This increase in area should indicate increasing lateral saturation of the rock fractured by sub-horizontal infiltrations, however, there is a clear connection of the areas of low resistivity.

The 610 m altitude map corresponds to a 34 m depth and coincides with the contact between the Irati (upper) and Tatuí (lower) Formations, described in a geological field survey (Fig. 4). This map shows several smaller areas with resistivity below 13 $\Omega$ .m, disconnected and independent, either in the center or in zones bordering the 50 $\Omega$ .m area. This diffusion of low resistivity zones must be conditioned to the occurrence of fine sandstones, porous rocks that allow three-dimensional flow of fluids.

**Fig. 8** Electrical resistivity maps for different depths



The maps at 600 m and 590 m altitude, or respectively at 44 m and 54 m depth, are characterized by their similarity to the 610 m map and by the increase in areas with resistivity below  $13\Omega.m$ , in addition to the increase in areas of high resistivity (above of  $50\Omega.m$ ) (Fig. 8).

The connection between water accumulated in the topographic depression that constitutes the wetland with the local aquifer reveals the sensitivity of this environment to the management and use of the land in its area of influence, mainly regarding the use of fertilizers and agricultural defensives [67–70]. In view of the high risk of direct contamination of the aquifer source and the persistence of various agrochemical compounds over long periods, with emphasis on compounds with metals, it is fundamental to propose legislation aimed at preserving these areas, similarly to what exists in Brazil for spring areas and rivers.

## 4 Conclusion

The geological and geophysical data reveal the hydrogeological function of the wetland under study. Although the local substrate consists of siltstones and limestones of low permeability, it was possible to recognize preferential zones of vertical flow that make the interconnection between the water accumulated in the interior of the wetland, with fine sandstones that form a regional aquifer positioned at approximately 45 m deep.

The terrain morphology in the study area configures a closed basin or depression, where any surface runoff will have the wetland as a catchment basin. Land use in this basin is represented by sugarcane monoculture, an agricultural activity that involves fertilizers and pesticides to maintain productivity, in addition to the release of vinasse as a fertilizer complement and soil humidifier.

This type of land use in a closed catchment basin and with base level constituted by an aquifer recharge area and, therefore, of high environmental sensitivity, requires additional care in relation to the release of agrochemicals and fertilizers. The boundary between wetland and cropland is simply a dirt road, completely devoid of natural vegetation or buffer zone.

The study area consists of one of the few remnants of regional aquifer recharge, a system of fundamental importance in maintaining a minimum flow in hydrographic basins during periods of drought, with emphasis on the Corumbataí River, whose catchment is responsible for supplying 666,000 people. The population growth in this hydrographic basin will demand the increasing exploration of groundwater resource in the upcoming years.

With a view to preserving similar recharge areas and the quality of the surface and groundwater resources, it is highly recommended to manage the land with the least possible impact in terms of the release of chemical products, in addition to establishing a buffer zone for sediments around, in a similar way to what is recommended in Brazilian legislation regarding the need for recovery and preservation of riparian forest, springs such as springs and rivers. The absence of protective legislation implies the high environmental vulnerability of wetlands in Brazil.

The integration of geological and geophysical data resulted in a broad diagnosis regarding the vulnerability of an ecosystem particularly sensitive to environmental impacts. The intensive sugarcane agriculture around the wetland area devoid of vegetation or runoff damping structures in rainfall events makes the input of fertilizers, pesticides and vinasse a natural consequence of land use, with direct risks to the groundwater quality.

The versatility, speed, low logistical complexity and the degree of detail obtained in the results, allow us to recommend this set of methodologies in investigations of aquifer recharge zones in the most varied land use scenarios, from agricultural areas to regions of difficult.

**Acknowledgements** This work was funded by the São Paulo Research Foundation (Fundação de Amparo à Pesquisa do Estado de São Paulo—FAPESP), through the project entitled “Hydrology and environmental function of upland wetlands in the Depressão Periférica Paulista (Brazil)” (Process n° 2020/03207-9).

**Author contributions** CAM: Conceptualization, planning, data acquisition, data processing, interpretation and writing. VSR: Planning, acquisition, critical data analysis and writing. MAFH: Critical data analysis, writing and review. HM: Critical data analysis, writing and review. RM: Critical data analysis, writing and review. All authors read and approved the final manuscript.

**Data availability** All data generated or analysed during this study are included in this published article [and its supplementary information files].

## Declarations

**Competing interests** The authors declare no competing interests.

**Open Access** This article is licensed under a Creative Commons Attribution 4.0 International License, which permits use, sharing, adaptation, distribution and reproduction in any medium or format, as long as you give appropriate credit to the original author(s) and the source, provide a link to the Creative Commons licence, and indicate if changes were made. The images or other third party material in this article are included in the article's Creative Commons licence, unless indicated otherwise in a credit line to the material. If material is not included in the article's Creative Commons licence and your intended use is not permitted by statutory regulation or exceeds the permitted use, you will need to obtain permission directly from the copyright holder. To view a copy of this licence, visit <http://creativecommons.org/licenses/by/4.0/>.



## References

1. Varis O, Biswas AK, Tortajada C, Lundqvist J. Megacities and watermanagement. *Int J Water Resour Dev.* 2006;22(2):377–94. <https://doi.org/10.1080/07900620600684550>.
2. Sánchez-Román RM, Folegatti MV, González AMGO. Water resources assessment at piracicaba, capivari and jundiá river basins: a dynamic systems approach. *Water Resour Manag.* 2010;24:761–73. <https://doi.org/10.1007/s11269-009-9470-x>.
3. González AMGO, Sánchez-Román RM, Folegatti MV, Zolin CA. PCJ river basins' water availability caused by water diversion scenarios to supply metropolitan areas of São Paulo. *Water Resour Manag.* 2011;25:3371–86. <https://doi.org/10.1007/s11269-011-9860-8>.
4. Coelho CAS, Cardoso DHF, Firpo MAF. Precipitation diagnostics of an exceptionally dry event in São Paulo, Brazil. *Theor Appl Climatol.* 2016;125:769–84. <https://doi.org/10.1007/s00704-015-1540-9>.
5. Millington N. Producing water scarcity in São Paulo, Brazil: The 2014–2015 water crisis and the binding politics of infrastructure. *Polit Geogr.* 2018;65:26–34. <https://doi.org/10.1016/j.polgeo.2018.04.007>.
6. Mello K, Randhir T. Diagnosis of water crises in the metropolitan area of São Paulo: policy opportunities for sustainability. *Urban Water J.* 2018;15(1):53–60. <https://doi.org/10.1080/1573062X.2017.1395895>.
7. Empinotti VL, Budds J, Aversa M. Governance and water security: The role of the water institutional framework in the 2013–15 water crisis in São Paulo, Brazil. *Geoforum.* 2019;98:46–54. <https://doi.org/10.1016/j.geoforum.2018.09.022>.
8. Abatan AA, Tett SFB, Dong B, Cunningham C, Rudorff CM, Klingaman NP, Abreu RC. Drivers and physical processes of drought events over the State of São Paulo, Brazil. *Clim Dyn.* 2022;58:3105–19. <https://doi.org/10.1007/s00382-021-06091-2>.
9. COMPANHIA NACIONAL DE ABASTECIMENTO—CONAB. Série Histórica das Safras. Brasília, 2021. <https://www.conab.gov.br/info-agro/safras/serie-historica-das-safras>. Accessed 03 2023.
10. Palacios-Berechea MC, Palacios-Berechea R, Ensinas AV, Garrido-Gallego A, Modesto M, Nebra SA. Brazilian sugar cane industry—a survey on future improvements in the process energy management. *Energy.* 2022;259:124903. <https://doi.org/10.1016/j.energy.2022.124903>.
11. Mutton MA, Rossetto R, Mutton MJR. Agricultural use of Stillage, 423–440. In: Luis Augusto Barbosa Cortez (Coord.). *Sugarcane bioethanol—R&D for Productivity and Sustainability*, São Paulo: Edgard Blücher, 2014. [https://doi.org/10.5151/BlucherOA-Sugar-cane-SUGARCANEETHANOL\\_40](https://doi.org/10.5151/BlucherOA-Sugar-cane-SUGARCANEETHANOL_40)
12. CETESB. COMPANHIA DE TECNOLOGIA DE SANEAMENTO AMBIENTAL—CETESB. Vinhaça—Critérios e procedimentos para aplicação no solo agrícola. Norma P4.231. 2006. São Paulo, SP, 6p. [http://www.ana.gov.br/Salalmprensa/doc\\_oficina/Vinha%C3%A7a.pdf](http://www.ana.gov.br/Salalmprensa/doc_oficina/Vinha%C3%A7a.pdf). Accessed 03 2023.
13. Christofolletti CA, Escher JP, Correia JE, Marinho JFU, Fontanetti CS. Sugarcane vinasse: environmental implications of its use. *Waste Manag.* 2013;33(12):2752–61. <https://doi.org/10.1016/j.wasman.2013.09.005>.
14. Cruz RL, Righetto AM, Nogueira MA. Experimental investigation of soil and ground water impacts caused by vinasse disposal. *Water Sci Technol.* 1991;24(11):77–85. <https://doi.org/10.2166/wst.1991.0339>.
15. Silva MAS, Griebeler NP, Borges LC. Uso de vinhaça e impactos nas propriedades do solo e lençol freático. *Rev Bras Eng Agrícola Ambient.* 2007;11(1):45–52.
16. Gunkel G, Kosmol J, Sobral M, Rohn H, Montenegro S, Aureliano S. Sugar cane industry as a source of water pollution—case study on the situation in Ipojuca River, Pernambuco, Brazil. *Water Air Soil Pollut.* 2007;180:261–9. <https://doi.org/10.1007/s11270-006-9268-x>.
17. Fuess LT, Garcia ML. Implications of stillage land disposal: a critical review on the impacts of fertigation. *J Environ Manag.* 2014;145:210–29. <https://doi.org/10.1016/j.jenvman.2014.07.003>.
18. González L, Mejía M. Impact of Ferti-Irrigation with Vinasse on Groundwater Quality. *Irrig Drain.* 2015;64(3):400–7. <https://doi.org/10.1002/ird.1873>.
19. Ortégón GP, Arboleda FM, Candela L, Tamoh K, Valdes-Abellan J. Vinasse application to sugar cane fields. Effect on the unsaturated zone and groundwater at Valle del Cauca (Colombia). *Sci Total Environ.* 2016;539:410–9. <https://doi.org/10.1016/j.scitotenv.2015.08.153>.
20. Hoarau J, Caro Y, Grondin I, Petit T. Sugarcane vinasse processing: toward a status shift from waste to valuable resource. A review. *J Water Process Eng.* 2018;24:11–25. <https://doi.org/10.1016/j.jwpe.2018.05.003>.
21. Silva JJ, Silva BF, Stradiotto NR, Petrović M, Gros M, Gago-Ferrero P. Identification of organic contaminants in vinasse and in soil and groundwater from fertigated sugarcane crop areas using target and suspect screening strategies. *Sci Total Environ.* 2021;761:143237. <https://doi.org/10.1016/j.scitotenv.2020.143237>.
22. Mitsch WJ, Gosselink JG. *Wetland.* 2nd ed. New York: Wiley; 1993. p. 722.
23. Junk W, Piedade MTF, Lourival R, Wittmann F, Kandus P, Lacerda LD, Schöngart J. Brazilian wetlands: their definition, delineation, and classification for research, sustainable management, and protection. *Aquatic Conserv.* 2014;24:5–22. <https://doi.org/10.1002/aqc.2386>.
24. Gloeden E, Cunha RCA, Fraccaroli MJB, Cleary RW. The behaviour of vinasse constituents in the unsaturated and saturated zones in the botucatu aquifer recharge area. *Water Sci Technol.* 1991;24(11):147–57. <https://doi.org/10.2166/wst.1991.0347>.
25. Van der Kamp G, Hayashi M. The groundwater recharge function of small wetlands in the Semi-Arid Northern Prairie. *Great Plains Res.* 1998;8:39–56.
26. Fleischmann A, Siqueira V, Paris A, Collischonn W. Modelling hydrologic and hydrodynamic processes in basins with large semi-arid wetlands. *J Hydrol.* 2018;561:943–59. <https://doi.org/10.1016/j.jhydrol.2018.04.041>.
27. Rosolen VS, Bueno GT, Mutema M, Moreira CA, Faria Junior IR, Nogueira G, Chaplot V. On the link between soil hydromorphy and geomorphological development in the Cerrado (Brazil) wetlands. *CATENA.* 2019;176:197–208. <https://doi.org/10.1016/j.catena.2019.01.022>.
28. Casagrande MFS, Furlan LM, Moreira CA, Rosa FTG, Rosolen V. Non-invasive methods in the identification of hydrological ecosystem services of a tropical isolated wetland (Brazilian study case). *Environ Challenges.* 2021;5:100233. <https://doi.org/10.1016/j.envc.2021.100233>.
29. Perdomo S, Kruse EE, Ainchil JE. Estimation of hydraulic parameters using electrical resistivity tomography (ERT) and empirical laws in a semi-confined aquifer. *Near Surf Geophys.* 2018;16:627–41. <https://doi.org/10.1002/nsg.12020>.

30. Furlan LM, Rosolen V, Moreira CA, Bueno GT, Ferreira ME. The interactive pedological-hydrological processes and environmental sensitivity of a tropical isolated wetland in the Brazilian Cerrado. *SN Appl Sci.* 2021;3(2):1–15. <https://doi.org/10.1007/s42452-021-04174-7>.
31. Sendrós A, Himi M, Lovera R, Rivero L, Garcia-Artigas R, Urruela A, Casas A. Geophysical characterization of hydraulic properties around a managed aquifer recharge system over the Llobregat River Alluvial Aquifer (Barcelona Metropolitan Area). *Water.* 2020;12(12):3455. <https://doi.org/10.3390/w12123455>.
32. Winter TC. Relation of streams, lakes, and wetlands to groundwater flow systems. *Hydrogeol J.* 1999;7:28–45. <https://doi.org/10.1007/s100400050178>.
33. Tomer MD, Schilling KE. A simple approach to distinguish land-use and climate-change effects on watershed hydrology. *J Hydrol.* 2009;376(1–2):24–33. <https://doi.org/10.1016/j.jhydrol.2009.07.029>.
34. Tu J. Combined impact of climate and land use changes on streamflow and water quality in eastern Massachusetts, USA. *J Hydrol.* 2009;379(3–4):268–83. <https://doi.org/10.1016/j.jhydrol.2009.10.009>.
35. Noretto MD, Jobbágy EG, Brizuela AB, Jackson RB. The hydrologic consequences of land cover change in central Argentina. *Agr Ecosyst Environ.* 2012;154(1):2–11. <https://doi.org/10.1016/j.agee.2011.01.008>.
36. Onia SK, Futter MN, Molot LA, Dillon PJ, Crossman J. Uncertainty assessments and hydrological implications of climate change in two adjacent agricultural catchments of a rapidly urbanizing watershed. *Sci Total Environ.* 2014;473–474(1):326–37. <https://doi.org/10.1016/j.scitotenv.2013.12.032>.
37. Vanella D, Ramírez-Cuesta JM, Sacco A, Longo-Minnolo G, Cirelli GI, Consoli S. Electrical resistivity imaging for monitoring soil water motion patterns under different drip irrigation scenarios. *Irrig Sci.* 2020. <https://doi.org/10.1007/s00271-020-00699-8>.
38. González R, Marín LE, Córdoba G. Hydrogeology and groundwater pollution of Yaqui Valley Sonora, Mexico. *Geof Int.* 1997. <https://doi.org/10.22201/igeof.00167169p.1997.36.1.624>.
39. Steinich B, Pacheco J, Escolero OA. Hydrogeology of a contaminated sole-source karst aquifer, Mérida, Yucatán, Mexico. *Geof Int.* 2000. <https://doi.org/10.22201/igeof.00167169p.2000.39.4.246>.
40. Redhaounia B, Ilondo BO, Gabtni HH, Sami H, Bédir M. Electrical resistivity tomography (ERT) applied to karst carbonate aquifers: case study from Amdoun, Northwestern Tunisia. *Pure Appl Geophys.* 2016;173:1289–303. <https://doi.org/10.1007/s00024-015-1173-z>.
41. Ebong ED, Akpan AE, Emeka CN, Urang JG. Groundwater quality assessment using geoelectrical and geochemical approaches: case study of Abi area, southeastern Nigeria. *Appl Water Sci.* 2017;7(5):2463–78. <https://doi.org/10.1007/s13201-016-0439-7>.
42. Loera HL, Leal JAR, Harris PD, Gaytan DET, Ruiz VJM, Gogichaishvili A. Geophysical exploration of fractured-media aquifers at the Mexican Mesa Central: satellite City, San Luis Potosí, Mexico. *Surv Geophys.* 2015;36:167–84. <https://doi.org/10.1007/s10712-014-9302-2>.
43. Sonkamble S, Sahya A, Jampani M, Ahmed S, Amerasinghe P. Hydro – geophysical characterization and performance evaluation of natural wetlands in a semi-arid wastewater irrigated landscape. *Water Res.* 2019;148:176–87. <https://doi.org/10.1016/j.watres.2018.10.040>.
44. Helene LPI, Moreira CA, Bovi R. Identification of leachate infiltration and its flow pathway in landfill by means of electrical resistivity tomography (ERT). *Environ Monit Assess.* 2020;192:249. <https://doi.org/10.1007/s10661-020-8206-5>.
45. Araffa SAS, Alrefaee HA, Nagy M. Potential of groundwater occurrence using geoelectrical and magnetic data: a case study from south Wadi Hagul area, the northern part of the Eastern Desert, Egypt. *J Afr Earth Sci.* 2020;172:103970. <https://doi.org/10.1016/j.jafrearsci.2020.103970>.
46. Ibraheem IM, Tezkan B, Bergers R. Integrated Interpretation of Magnetic and ERT Data to Characterize a Landfill in the North-West of Cologne, Germany. *Pure Appl Geophys.* 2012;178:2127–48. <https://doi.org/10.1007/s00024-021-02750-x>.
47. Othman AA, Beshr AM, Ahmed MS, El-Gawad A, Ibraheem IM. Hydrogeophysical investigation using remote sensing and geoelectrical data in southeast Hiw, Qena, Egypt. *Geocarto Int.* 2022. <https://doi.org/10.1080/10106049.2022.2087750>.
48. Moreira CA, Helene LPI. Identification for a favorable area of groundwater exploitation based on structural and geoelectrical data in fractured aquifer in Southern Brazil. *Geof Int.* 2022. <https://doi.org/10.22201/igeof.00167169p.2022.61.4.2045>.
49. PCJ. Relatório institucional da agência das bacias PCJ. Fundação agência das bacias hidrográficas dos rios Piracicaba, Capivari e Jundiá. Piracicaba, 70p., 2020. <https://agencia.baciaspcj.org.br/institucional2020/wp-content/uploads/2021/04/Relatorio-Institucional-da-Agencia-das-bacias-PCJ-2020.pdf>. Accessed 03 2023.
50. Palmieri V, Carvalho RJ. Qual2e model for the Corumbataí River. *Ecol Model.* 2006;198(1–2):269–75. <https://doi.org/10.1016/j.ecolmodel.2006.04.018>.
51. Sánchez-Román RM, Folegatti MV, Orellana-González AMG. Water resources situation at piracicaba, capivari and jundiá watersheds using a dynamic systems model. *Engenharia Agrícola.* 2009;29(4):578–90.
52. Schneider RL, Muhlmann H, Tommasi E, Medeiros RA, Daemon RF, Nogueira AA. Revisão estratigráfica da Bacia do Paraná. *Congresso Brasileiro de Geologia*, 28, Porto Alegre, Sociedade Brasileira de Geologia. 1974;1:41–65.
53. Zalán PV, Wolf S, Conceição JJC, Astolfi MAM, Vieira IS, Appi VT, Zanatto OA. Tectônica e Sedimentação da Bacia do Paraná. *Simpósio Sul Brasileiro de Geologia*, 3., Curitiba, Sociedade Brasileira de Geologia. 1987;1:441–477.
54. Gama E Jr, Bandeira AN Jr, França AB. Distribuição espacial e temporal das unidades litoestratigráficas paleozóicas na parte central das Bacia do Paraná. *RBG.* 1982;12(4):578–89.
55. Santos RV, Souza PA, Alvarenga CJS, Dantas EL, Pimentel MM, Oliveira CG, Araújo LM. Shrimp U-Pb zircon dating and palynology of bentonitic layers from the Permian Irati Formation, Paraná Basin, Brazil. *Gondwana Res.* 2006;9(4):456–63. <https://doi.org/10.1016/j.jgr.2005.12.001>.
56. Soares PCO. limite glacial/pós-glacial do Grupo Tubarão no Estado de São Paulo. *An Acad Bras Ciênc.* 1972;44:333–42.
57. Fulfaro VJ, Saad AR, Santos MV, Vianna RB. Compartimentação e evolução tectônica da bacia do Paraná. *RBG.* 1982. <https://doi.org/10.25249/0375-7536.1982124590611>.
58. Secretaria do Meio Ambiente—SMA. As águas subterrâneas do Estado de São Paulo. Governo de Estado de São Paulo-SMA, 106p. 2014. <http://arquivo.ambiente.sp.gov.br/cea/2014/11/01-aguas-subterraneas-estado-sao-paulo.pdf>. Accessed 03 2023.
59. Milson J, Eriksen A. *Field geophysics*. 4th ed. Chichester: John Wiley & Sons; 2011. p. 304 ([10.1002/9780470972311](https://doi.org/10.1002/9780470972311)).
60. Kirsch R. *Groundwater geophysics: a tool for hydrogeology*. 2nd ed. Heidelberg: Springer; 2009. p. 556 ([10.1007/978-3-540-88405-7](https://doi.org/10.1007/978-3-540-88405-7)).
61. Abem AI. *Terrameter LS Instruction Manual*. Sundbyberg: ABEM Instrument Sundbyberg; 2012. p. 122.

62. Geotomo Software. Geoelectrical Imaging 2D & 3D—RES2DINV, ver. 3.52 for Windows 98/Me/2000/NT/XP. Rapid 2D resistivity & IP inversion using the least-squares method. Malaysia: Geotomo Software; 2003. p. 125.
63. Loke MH, Barker R. D Rapid least-squares inversion of apparent resistivity pseudosections by a quasi-Newton method. *Geophys Prospect*. 1996;44(1):131–52. <https://doi.org/10.1111/j.1365-2478.1996.tb00142.x>.
64. Ammar AI, Kamal KA, El-Boghdady MFM. 2D and 3D visualization of aquifer sediments, surface water seepage and groundwater flow using DC-resistivity, DC-IP, and SP methods, West El-Minia, Egypt. *Environ Earth Sci*. 2023;82:21. <https://doi.org/10.1007/s12665-022-10697-y>.
65. Cortês ARP, Moreira CA, Sampaio Paes RA, Veloso DIK. Geophysical and metallogenetic modelling of the copper occurrence in Camaqua Sedimentary Basin, Brazilian Southern. *Pure Appl Geophys*. 2019;176:4955–68. <https://doi.org/10.1007/s00024-019-02190-8>.
66. Bovi R, Moreira CA, Rosolen VS, Rosa FTG, Furlan LM, Helene LPI. Pipping process: genesis and network characterization through a pedological and geophysical approach. *Geoderma*. 2020. <https://doi.org/10.1016/j.geoderma.2019.114101>.
67. Li L, Liu W, Zhang X, Zheng F. Impacts of land use change and climate variability on hydrology in an agricultural catchment on the Loess Plateau of China. *J Hydrol*. 2009;377(1–2):35–42. <https://doi.org/10.1016/j.jhydrol.2009.08.007>.
68. Sophocleus M. Interactions between groundwater and surface water: the state of the art. *Hydrogeol J*. 2002;10(1):52–67. <https://doi.org/10.1007/s10040-001-0170-8>.
69. Santos RMB, Sanches Fernandes LF, Moura JP, Pereira MG, Pacheco FAL. The impact of climate change, human interference, scale and modeling uncertainties on the estimation of aquifer properties and river flow components. *J Hydrol*. 2014;519:1297–314. <https://doi.org/10.1016/j.jhydrol.2014.09.001>.
70. McLaughlin D, Kaplan DA, Cohen MJ. A significant nexus: geographic isolated wetlands influence landscape hydrology. *Water Resource Research*. 2014;50:7153–66. <https://doi.org/10.1002/2013WR015002>.

**Publisher's Note** Springer Nature remains neutral with regard to jurisdictional claims in published maps and institutional affiliations.